Journal of Materials Chemistry B

Accepted Manuscript

ROYAL SOCIETY OF CHEMISTRY

www.rsc.org/materialsB

Lacritin-mediated regeneration of the corneal epithelia by protein polymer nanoparticles

Wan Wang[1], Jordan Despanie[1], Pu Shi[1], Maria C. Edman-Woolcott[1], Yi-An Lin[4], Honggang Cui[4], J. Martin Heur[5], M. Elizabeth Fini[6], Sarah F. Hamm-Alvarez[1,2], and J. Andrew MacKay[1,3]

[1]Department of Pharmacology and Pharmaceutical Sciences, University of Southern California Los Angeles, CA; 90033-9121
[2]Department of Physiology and Biophysics, Keck School of Medicine of the University of Southern California, Los Angeles, CA; 90033-9121
[3]Department of Biomedical Engineering, University of Southern California, Los Angeles, CA; 90033
[4]Department of Chemical and Biomolecular Engineering, Johns Hopkins University, Baltimore, MD; 21218
[5]Department of Ophthalmology, Keck School of Medicine of the University of Southern California, Los Angeles, CA; 90033-9121
[6]Institute for Genetic Medicine, Keck School of Medicine of the University of Southern California, Los Angeles, CA; 90033-9121
Corresponding author: MacKay, J. Andrew (jamackay@usc.edu)
Address: Department of Pharmacology and Pharmaceutical Sciences, University of Southern California; Los Angeles, CA; 90033-9121. Phone Number: 323-442-4118

Manuscript Information: Title: 10 words; Abstract: 242 words; Text: 4,519 words; Figures: 7; Tables: 1; References: 52.

Abbreviations: Elastin-like polypeptides (ELPs), transition temperature (T_t), critical micelle temperature (CMT), SV40-Adeno vector transformed human corneal epithelial cell (HCE-T), non-obese diabetic (NOD), Bovine Pituitary Extract (BPE), Epidermal Growth Factor (EGF).

Keywords: Elastin-like polypeptide (ELPs), Lacritin, wound healing, nanoparticle, cornea

Abstract

The avascular corneal epithelium plays an important role in maintaining normal vision and protecting the corneal interior from environmental infections. Delayed recovery of ocular wounds caused by trauma or refractive surgery strengthens the need to accelerate corneal wound healing and better restore the ocular surface. To address this need, we fused elastin-like polypeptide (ELP) based nanoparticles SI with a model mitogenic protein called lacritin. Lacritin fused at the N-terminus of the SI diblock copolymer is called LSI. This LSI fusion protein undergoes thermo-responsive assembly of nanoparticles at physiologically relevant temperatures. In comparison to ELP nanoparticles without lacritin, LSI showed potent signs of lacritin specific effects on a human corneal epithelial cell line (HCE-T), which included enhancement of cellular uptake, calcium-mediated signaling, and closure of a scratch. *In vivo*, the corneas of non-obese diabetic mice (NOD) were found to be highly responsive to LSI. Fluorescein imaging and corneal histology suggested that topical administration of LSI onto the ocular surface significantly promoted corneal wound healing and epithelial integrity compared to mice treated with or without plain ELP. Most interestingly, it appears that ELP-mediated assembly of LSI is essential to produce this potent activity. This was confirmed by comparison to a control lacritin ELP fusion called LS96, which does not undergo thermally-mediated assembly at relevant temperatures. In summary, fusion of a mitogenic protein to ELP nanoparticles appears to be a promising new strategy to bioengineer more potent biopharmaceuticals with potential applications in corneal wound healing.

1. Introduction

Eye injury is reported to be the second most common cause of visual impairment in the United States after cataracts.[1] Back in 2006, emergency room (ER) visits for eye injuries represented 1.4% of all ER visits.[1] To maintain corneal transparency and rigidity, the corneal epithelium serves as an important barrier between the external environment and the delicate internal ocular tissues.[2] Although the corneal epithelium normally recovers rapidly from damage, certain clinical conditions including diabetic retinopathy, herpes simplex virus infection, neurotrophic keratopathy, and corneal transplants result in delayed wound healing, often precipitating sight-threatening complications.[3] Thus, there remains a need for more effective therapies to facilitate epithelial healing on the ocular surface. Moreover, recovery times following popular refractive procedures, such as photorefractive keratectomy (PRK) and laser in situ keratomileusis (LASIK), directly rely on the patients' corneal wound healing response; however these procedures may lead to haze, dry eye disease, nerve damage, and Diffuse Lamellar Keratitis (DLK).[4]

Corneal epithelium recovery after injury involves apoptosis, migration, proliferation, and differentiation of multiple cells in a cascade mediated by cytokines, growth factors, and chemokines.[3] Naturally present in the anterior segment of the eye and responsible for the migration and proliferation of corneal epithelial cells, growth factors have become a class of promising therapeutic candidates in treating visual impairments.[5] An enhanced wound healing effect has been observed in primate models and clinical trials via topical treatment with epidermal growth factor (EGF),[6, 7] keratinocyte growth factor,[8] nerve growth factor,[9] etc. As such, it would be of great clinical value to rationally bioengineer growth factor-like proteins into therapies using a robust formulation process. Successful earlier trials include increased tensile strength of full thickness corneal wounds after topical epidermal growth factor (EGF) treatment[10] and better ulcer healing in diabetic patients from platelet-derived growth factor-BB (PDGF-BB) in a topical gel formulation.[11] One novel candidate to stimulate wound healing on the ocular surface is the mitogen known as lacritin.[12] Lacritin is the most severely downregulated protein in contact lens related dry eye and is similarly deficient in blepharitis (a common inflammation of the eyelid).[13] Previous *in vitro* tests have shown that, on the ocular surface, lacritin triggers Ca^{2+} wave propagation,[13] in addition to promoting the survival of primary and cultured human corneal epithelial cells stressed with interferon-γ, tumor necrosis factor[14], and Benzalkonium chloride (BAK),[15] indicative of both mitogenic and cytoprotective activity. This cell targeting specificity is triggered by a unique 'off-on' switch controlled by heparanase deglycanation of the cell surface protein, syndecan-1, which exposes a lacritin binding site as a prerequisite for its downstream mitogenic signaling.[16, 17]

Although topical application of ophthalmic products has remained the most popular and well-tolerated administration route for patient compliance, the bioavailability of eye drops is severely hindered by blinking, baseline and reflex lachrymation, and nasolacrimal drainage.[18] One solution to enhancing the therapeutic index of topical treatments is through the application of polymeric nanoparticles as drug carriers.[19-21] Polymeric nanoparticles displaying therapeutic ligands at the corona can interact with complex biomolecular architectures through multiple simultaneous interactions (multivalency) and exhibit the well-defined sizes required for efficient tissue penetration.[22] One such material capable of being employed as the scaffold are thermo-responsive elastin-like polypeptides (ELPs).[23] ELPs are composed of the repetitive pentapeptide motif (Val-Pro-Gly-*Xaa*-Gly)$_n$ and exhibit unique reversible inverse phase transition temperatures, T_t, below which they solubilize and above which they phase separate.[24] T_t can be modulated through guest residue (*Xaa*) selection and changes in the number of pentameric repeats, n.[25, 26] We have previously reported the successful bioengineering of diblock ELP nanoparticles to suppress tumor growth with rapamycin binding at both the corona as well as in the core;[27] uptake of ELP nanoparticles displaying adenovirus knob domain into hepatocytes and acinar cells has also been described.[28] Moreover, Callahan and coworkers have demonstrated enhanced intratumoral spatial distribution of ELP nanoparticles via triple stimuli[29] while MacEwan and coworkers observed controlled cellular uptake in HeLa, MCF7, and primary HUVEC cells using local Arg density modulation on ELP nanoparticles.[30] Collectively, these studies illustrate the potential of ELP nanoparticles to enhance both local and systemic therapeutic effects as a drug carrier.

Inspired by the motivation to further explore lacritin's function on the ocular surface, enhance its bioavailability, and better target the corneal epithelium, we utilized a diblock ELP (SI) nanoparticle scaffold to bioengineer LSI nanoparticles with multivalent presentation of lacritin at the surface (Table 1). The thermo-responsiveness and self-assembly of LSI nanoparticles was investigated by UV-Vis turbidity analysis, dynamic light scattering (DLS), and transmission electron microscopy (TEM). LSI exhibited mitogenic activity *in vitro* as confirmed by Ca^{2+} wave propagation and scratch wound healing using SV40-transduced human corneal epithelial cells (HCE-Ts). To further explore the *in vivo* efficacy of LSI nanoparticles, we created abrasion wounds on the ocular surface of female NOD mice mimicking the PRK procedure and topically treated the eye with two doses of LSI nanoparticles within 12 h after the surgery. The LSI treated group exhibited significantly faster wound healing compared to SI, epidermal growth factor (EGF), and bovine pituitary extract (BPE) co-treatment, and no treatment. To address the importance of multivalency, we also included a control lacritin ELP fusion that does not undergo thermally mediated assembly, called LS96. Murine corneal abrasion recovery study strongly supported enhanced healing efficacy of LSI nanoparticles over LS96 in a 12 h timeframe. Histology analysis revealed that, after LSI treatment, no significant corneal inflammation was observed and the reconstituted ocular surface appeared as smooth as pre-procedure following 24 h. For the first time, we have successfully bioengineered multivalent self-assembling LSI nanoparticles based on the thermo-responsive SI nanoparticle scaffold, confirmed its *in vitro* mitogenic activity using HCE-Ts, and corroborated the efficacy using a novel murine corneal abrasion model. This report provides the first *in vivo* verification of lacritin's wound healing potential and can be further applied to rationally bioengineer other peptide therapeutics into self-assembling nanoparticles for treating visual impairments using the ELP delivery system.

2. Materials and Methods

2.1. Materials and equipment

TB DRY® Powder Growth Media was purchased from MO BIO Laboratories, Inc. (Carlsbad, CA). NHS-Rhodamine was purchased from Thermo Fisher Scientific (Rockford, IL). SV40-Adeno vector transformed cornea cells (RCB 2280, HCE-T) were purchased from Riken Cell Bank, Japan. Keratinocyte-SFM medium supplied with Bovine Pituitary Extract (BPE) and prequalified human recombinant Epidermal Growth Factor 1-53 (EGF) was purchased from Gibco Invitrogen (Life Technologies, NY). Calcium Indicator Fluo-4, AM, cell permeant was purchased from Life Technologies (NY). Algerbrush II with a 0.5 mm burr was purchased from The Alger Company, Inc., TX. *In vivo* studies were conducted using 12-week female non-obese diabetic (NOD) (Taconic Farms, Germantown/NY, USA) mice. All procedures performed were in accordance with IACUC approval and oversight.

2.2. Construction of LSI nanoparticles

Genes encoding for ELPs (SI) were synthesized by recursive directional ligation in pET25b(+) vector as previous reported.[27] A sequence encoding human lacritin without secretion signal peptide was designed using the best *E. coli* codons in EditSeq (DNAStar Lasergene, WI). A thrombin cleavage site was designed between the lacritin sequence and ELP tag via insertion at the *BseRI* site. Lacritin gene flanked by *NdeI* and *BamHI* restriction digestions sites at the 5' and 3' ends was purchased in the pIDTSmart-KAN vector from Integrated DNA Technologies (IDT) as follows:

5'-

CATATGGAAGACGCTTCTTCTGACTCTACCGGTGCTGACCCGGCTCAGGAAGCTGGTACCTCTAAACCGA
ACGAAGAAATCTCTGGTCCGGCTGAACCGGCTTCTCCGCCGGAAACCACCACCACCGCTCAGGAAACCT
CTGCTGCTGCTGTTCAGGGTACCGCTAAAGTTACCTCTTCTCGTCAGGAACTGAACCCGCTGAAATCTATC
GTTGAAAAATCTATCCTGCTGACCGAACAGGCTCTGGCTAAAGCTGGTAAAGGTATGCACGGTGGTGTTC
CGGGTGGTAAACAGTTCATCGAAAACGGTTCTGAATTCGCTCAGAAACTGCTGAAAAAATTCTCTCTGCTG
AAACCGTGGGCTGGTCTGGTTCCGCGTGGTTCTGGTTACTGATCTCCTC**GGATCC-**3'.

The above gene was subcloned into the pET25b(+) vector and the LSI gene was synthesized by ligation of ELP SI gene via the *BseRI* restriction site. Correct cloning of the fusion protein gene was confirmed by DNA

sequencing. LSI fusion proteins were expressed in BLR (DE3) *E. coli* (Novagen Inc., Milwaukee, WI) for 24 h in an orbital shaker at 37 °C at 250 rpm and purified via inverse phase transition cycling as previously reported.[31]

2.3. Characterization of LSI phase behavior and nanoparticle formation

The phase diagram for LSI fusion protein was characterized by optical density change at 350 nm as a function of solution temperature using a DU800 UV-VIS Spectrophotometer (Beckman Coulter, Brea, CA). T_t was defined at the point of the maximum first derivative. Self-assembly of nanoparticles was measured using dynamic light scattering (DLS) using a DynaPro-LSR Plate Reader (Wyatt Technology, Santa Barbara, CA). Light scattering data were collected at regular temperature intervals (1 °C) as solutions were heated from 5 to 50 °C. The results were analyzed using a Rayleigh sphere model and fitted into a cumulant algorithm based on the sum-of-squares value. The critical micelle temperature (CMT) was defined as the lowest temperature at which the R_h is significantly greater than the average monomer R_h.

2.4. TEM imaging of LSI nanoparticles

The TEM imaging was carried out on a FEI Tecnai 12 TWIN microscope (Hillsboro, OR) at 100 kV. Briefly, a 100 μM solution (5 μL) was initially deposited on a copper grid with carbon film (CF400-Cu, Election Microscopy Sciences, Hatfield, PA). After removing the excess amount of solution with filter paper, the samples were negatively stained with 2 % uranyl acetate, followed by removing excess uranyl acetate after 30 s. The samples were then dried under room temperature for at least 3 h before use in imaging.

2.5. SV40-immortalized human corneal epithelial cell (HCE-T) culture

SV40-immortalized HCE-T cells (Riken Cell Bank, Japan) were grown in keratinocyte-SFM media (KSFM, Life Technologies, Rockville, MD) containing bovine pituitary extract (BPE, 50 μg/ml) and epidermal growth factor (EGF, 5 ng/ml). Cell passages 4-6 were used for Ca^{2+} imaging, scratch and uptake assays in 35-mm coverslip-bottomed dishes. To optimize responsiveness upon stimuli, cells were starved with EGF and BPE free medium for 24 h before experimentation.

2.6. Ca^{2+} imaging

HCE-Ts were rinsed twice with Ca^{2+} and Mg^{2+} free phosphate buffer saline (PBS) and incubated at 37 °C for 20 m in fresh KSFM medium containing 2.5 μM calcium probe Fluo-4 AM (Invitrogen Life technologies, NY). The cells were then rinsed twice with NaCl Ringer buffer (145 mM NaCl, 5 mM KCl, 1 mM $CaCl_2$, 1 mM KH_2PO_4, 1 mM $MgCl_2$, 10 mM glucose, and 10 mM HEPES, osmolarity 300, pH 7.4) and kept in the same buffer at room temperature for 30 m. For Ca^{2+} free medium, 1 mM Ca^{2+} was replaced with 0.5 mM EGTA. The cells were illuminated at 488 nm, and their emission was monitored every 3.15 s at 510 nm using Zeiss LSM 510 Meta confocal microscope system. The field of interest contained 24 to 45 cells, and the fluorescent intensity change was calculated for each region with image-analysis software. Ca^{2+} dynamics were evaluated using the changes in fluorescence intensity of Fluo-4AM. The data are presented as percentage change in fluorescence intensity at each time point (F_t) to the first time point (F_0) reading: $(F_t-F_0)/F_0\times100\%$.

2.7. *In vitro* scratch closure assay

For a scratch assay, confluent HCE-T monolayers were scraped in a straight line to create a scratch wound with a p200 pipet tip.[32] Cells were rinsed with KSFM medium without BPE or EGF to remove debris and then incubated with fresh KSFM medium containing BPE (50 μg/ml) and EGF (5 ng/ml), LSI, or medium without growth factors (No treat). Phase contrast images of the wound at the beginning and after 24 h treatment were captured using Zeiss LSM 510 Meta confocal microscope system.

2.8. Exogenous cell uptake assay

SI and LSI nanoparticles were conjugated with NHS-Rhodamine (Thermo Fisher Scientific Inc, Rockford, IL) via covalent modification of the amino terminus. Conjugation was performed in 100 mM borate buffer (pH 8.0)

for 2 h (LSI) or overnight (SI) at 4 °C followed by desalting on a PD10 column (GE Healthcare, Piscataway, NJ) to remove free dye. Briefly, after the cells were rinsed with fresh medium without BPE and EGF, 10 μM rhodamine labeled proteins were added into the dish. After incubation at 37 °C for different time points, the cells were rinsed and images were acquired using Zeiss LSM 510 Meta confocal microscope system.

2.9. Murine corneal abrasion and recovery study

Briefly, 12-week female NOD mice were anesthetized with an i.p. injection of xylaxine/ketamine (60-70 mg+5 mg/kg) and placed on a heating pad. After cleaning the ocular surface with eye wash (OCuSOFT, INC., TX), the corneal epithelium of the right eye was removed down to the basement membrane using an algerbrush II (The Alger Company, Inc., TX); the left eye was left intact as a contra lateral control. Mice were allowed to heal for 24 h with 2 doses (5 μl) of KSFM medium containing BPE (50 μg/ml) and EGF (5 ng/ml), 100 μM LSI, 100 μM SI, or no treatment at 12 h intervals. After staining the ocular surface with 5 μl 0.6 mg/ml fluorescein (Akorn, IL), images of the abrasion wound were captured using a Moticam 2300 camera after 12 h and 24 h.

2.10. Statistics

All experiments were replicated at least three times. Maximum fluorescence intensity change in Ca^{2+}-mediated fluorescence was analyzed using a non-paired t-test. Scratch wound healing quantification was analyzed using a one-way ANOVA followed by Tukey's post-hoc test. HCE-T uptake was analyzed using two-way ANOVA followed by Bonferroni post-test and murine corneal epithelium recovery from abrasion wound were analyzed using Kruskal-Wallis non-parametric ANOVA. Corneal wound healing comparison between LSI and LS96 after 12 h treatment was analyzed using Mann-Whitney U test. A p value less than 0.05 was considered statistically significant.

3. Results and discussion

3.1. The ELP lacritin fusion called LSI forms thermo-responsive nanoparticles

Lacritin moderates homeostasis through receptor-mediated events across the anterior segment of the eye.[12] In principle, it is possible to further enhance the activity of receptor-mediated events through the deliberate formation of multivalent protein polymer nanoparticles (Fig. 1A).[28, 33, 34] While targeting ligands have been explored using ELP based nanoparticles similar to SI (Table 1), to the best of our knowledge, this approach has never been used to modulate the activity of a cell signaling protein such as lacritin. To explore this possibility, LSI and LS96 (Table 1) were cloned into a pET25(+) vector, expressed in *E. coli*, and purified using inverse phase transition cycling (Fig. 1B). As shown in Fig. 1A, a chemically synthesized gene encoding lacritin was fused to the ELP diblock copolymer called SI and expressed as a fusion protein called LSI. LSI was expected to undergo thermally-mediated assembly similar to SI and form nanoparticles above its phase transition temperature (T_t), while LS96, with lacritin gene fused to the soluble macromolecule S96, was developed as a control that does not phase separate until significantly above physiological temperatures. After confirming the purity and molecular weight of expressed proteins, their phase diagrams were characterized using optical density as a function of temperature (Fig. 1C). While monomeric ELPs undergo a single phase transition from solubility to coacervate, certain ELP diblock copolymers display two steps of assembly in response to heating: i) soluble monomers assemble into stable nanoparticles above T_{t1}; and ii) at a higher temperature, T_{t2}, the nanoparticles themselves coacervate (Fig. 1D). For ELPs such as SI, T_{t1} is thus defined as the critical micelle temperature (CMT) above which nanoparticles are favorable (32.3 °C at 25 μM). T_{t2}, or the bulk phase transition temperature, represents the temperature at which these nanoparticles further assemble into coacervates.[35] In striking contrast to its SI scaffold, LSI only shows one phase transition at 18.4 °C (25 μM). Moreover, LSI illustrated less concentration dependent phase transition compared to the SI scaffold, as demonstrated by a decreased slope when T_t was fit by the equation:

$$T_t = m \log[C_{ELP}] + b, \qquad \text{Eq. 1.}$$

where C_{ELP} is the concentration, m is the slope, and b is the transition temperature at 1 μM (Fig. 1D). Eq. 1 permits the estimation of T_t over a broad range of concentrations, which may be encountered *in vivo*. In our

recent reports, suppression of the ELP concentration dependence correlates with assembly mediated by the fusion domain itself, which we have reported in fusion between a single chain antibody and also a disintegrin.[31]

Based on the unexpected observation that LSI exhibits a single phase transition, dynamic light scattering (DLS) was used to determine whether particles form above or below this T_t. Both constructs were thus compared by DLS to monitor the temperature dependent assembly process (Fig. 2A). Surprisingly, LSI preassembled into 30-40 nm nanoparticles even below T_t. Above T_t, it began to favor larger nanoparticles ranging from 130-140 nm. Consistent with our previous reports, SI remained as 20-30 nm micelles at physiologically relevant temperatures (Fig. 2A). In combination with the optical density data, this suggests that lacritin itself mediates partial assembly of small aggregates that proceed to assemble larger structures above the T_{t1} mediated by SI. To further examine the dominant structures formed by LSI and SI, we observed their morphologies when dried from room temperature using transmission electron microscopy (TEM). Consistent with DLS, while SI formed a mono-dispersed micelle structure with an average diameter of 36.5 ± 5.8nm (Fig. 2B) and LSI formed larger nanoparticles that exhibit average diameters of 67.1 ± 11.5nm (Fig. 2C). Regardless, both SI and LSI appear capable of forming nanostructures; therefore, we proceeded to investigate the potential for these lacritin functionalized nanoparticles to participate in lacritin-mediated signaling and healing relevant to the corneal epithelium.

3.2. LSI nanoparticles exhibit mitogenic activity using SV-40 transduced human corneal epithelial cells

Upon injury, one of the earliest reactions of many epithelial cells is a transient Ca^{2+} wave spreading across the monolayer cell sheet.[36] The Ca^{2+} wave triggers downstream signaling pathways responsible for cell migration, proliferation and other events associated with wound repair.[37, 38] Sanghi et al. first reported lacritin's ability to stimulate Ca^{2+} wave propagation throughout HCE-Ts while initially exploring its efficacy on the ocular surface.[13] Further studies have confirmed that this Ca^{2+} signal is associated with lacritin's protection of HCE cells stressed with BAK[15] and maintenance of cultured corneal epithelia homeostasis.[14] To confirm whether LSI maintains mitogenic activity of lacritin, we tested both calcium transients and scratch wound healing assays based on the reported HCE-T model.[39] We first tested intracellular Ca^{2+} wave propagation in HCE-T cells loaded with Fluo-4 AM under either LSI or SI treatment. The fields of interest containing 24 to 45 cells were chosen and the fluorescent intensity change of ten individual cells was calculated using LSM 510 image-analysis software. Percentage change in fluorescence intensity at each time point (F_t) to the first time point (F_0) reading: $(F_t-F_0)/F_0\times100\%$ was used to quantify Ca^{2+} signal. The signal triggered by SI was negligible, evoking only a 0.054 ± 0.049 fold maximum fluorescence intensity change compared to baseline. The addition of LSI nanoparticles, however, resulted in a significantly rapid calcium influx into the cells with a maximum fluorescence intensity 4.399 ± 1.043 fold of F_0 ($p<0.0001$, Fig. 3). Moreover, HCE-T cells appeared to have 'memory' for exogenous LSI treatment, as treating the same group of cells for the second time with the same concentration resulted in a broader peak for Ca^{2+} influx, which extended peak duration from 40 to 70 s (Fig. 3A). Downstream of Ca^{2+} mediated signaling,[40] HCE-Ts are known to initiate more rapid motility and proliferation,[14, 41] which can be visualized during the closure of a scratch made on a confluent sheet of cells. To visualize the *in vitro* effect of LSI, we applied a scratch to a sheet of cells and captured the time-lapse healing process (Fig. 4A). Each treatment was performed in triplicate and four independent wound distances in each well were measured for analysis. After 24 h of treatment, a very low concentration of LSI (10 nM) significantly accelerated scratch wound healing compared to plain medium without growth-factors (***$p<0.001$). This effect was comparable to a positive control containing BPE and EGF.

3.3. LSI nanoparticles undergo uptake into HCE-Ts

Encouraged by LSI's *in vitro* mitogenic activity, we further explored whether exogenous LSI can enter the HCE-Ts. The cells were thus incubated with NHS-rhodamine labeled LSI and SI nanoparticles for different time points and representative images were shown in Fig. 5. Consistent with lacritin-mediated uptake, LSI underwent cell uptake into HCE-Ts in a time dependent manner (Fig. 5A). Significant cell entry was observed

10 m following incubation, and after 1 h, LSI nanoparticles accumulated within the peri-nuclear region. Upon quantification, LSI exhibited significantly higher cytosolic fluorescence than SI nanoparticles ($p<0.0001$, Fig. 5B). Nanomaterials of different sizes, shapes, and charges have been widely used in biomedical imaging, tissue targeting, and cell uptake.[42-44] More recently, the use of nanoparticles to crosslink membrane receptors more efficiently to regulate downstream signaling has attracted enormous attention, especially in antibody mediated receptor crosslinking.[45, 46] This data suggests that LSI may be useful as a platform to not only stimulate lacritin-mediated mitogenesis, but could also have applications in the targeted delivery of other agents (antibodies, small molecules) to the cells of the cornea.

3.4. LSI nanoparticles heal a corneal abrasion on non-obese diabetic (NOD) mice

While evidence for lacritin's mitogenic activity have been confirmed,[14, 41] the *in vivo* mitogenic potential of lacritin has not been previously reported. As such, our *in vitro* results inspired us to investigate the activity of LSI nanoparticles on the ocular surface. To do so, we proceeded to investigate their *in vivo* efficacy via the easiest and most well-tolerated delivery approach- topical eye drops. In this study, we developed a corneal epithelial abrasion model on female NOD mice to assess the wound-healing effect of LSI nanoparticles. Non-obese diabetic (NOD) mice are frequently used as an animal model for impaired wound healing in humans. For example, Darby and coworkers have previously compared the skin wound healing process in non-obese diabetic (NOD) mice and C57BL/6 mice. Reduced cell proliferation, retarded onset of the myofibroblast phenotype, reduced procollagen I mRNA expression, and aberrant control of apoptotic cell death were observed in NOD group.[47] Alternatively, Rich and coworkers used NOD mice as an impaired wound healing model to study the pathogenesis of Staphylococcus aureus infection.[48] Also, Lee and coworkers have implanted alginate hydrogels loaded with model drug VEGF into NOD mice after femoral artery ligation to increase collateral circulation under cyclic mechanical stimulation.[49]

Based on the above reports, the NOD mouse model was selected for evaluation of the *in vivo* activity of LSI nanoparticles. Briefly, a circular abrasion wound with a diameter of around 2 mm was created on the right eye of the animal with an algerbrush II without damaging the limbal region.[50, 51] Immediately after imaging, 5 µl of 100 µM LSI nanoparticles, SI nanoparticles, or control EGF+BPE were topically administered to the ocular surface, and this treatment was repeated once 12 h after wound initiation. Images of the wound were captured at time 0, 12 h, and 24 h using fluorescein staining under cobalt blue light (Fig. 6A). The initial wound healing comparison study included 4 mice under each treatment group, with the left eye intact as a contralateral control. After experimentation, wound-healing images were analyzed using ImageJ. Mean fluorescein intensity, wound area, total fluorescein (total=mean fluorescein intensity × wound area), fluorescein percentage of initial value, wound area percentage of initial value (PctArea), and total fluorescein percentage of initial value were determined by a blind reviewer and compared between groups at 12 h and 24 h using Kruskal-Wallis non-parametric testing. No significant inflammation or any other adverse effects were observed upon treatments. Notably, LSI at both 12 and 24 hours significantly decreased the percentage of initial wound area (PctArea) compared to SI ($p=0.001$), EGF+BPE ($p=0.001$), and no treatment groups ($p=0.001$), suggesting that LSI is the best formulation to accelerate recovery of the corneal epithelium (Fig. 6B). To corroborate the fluorescein imaging result, we further processed the corneal epithelium after 24 h for histology analysis (Fig. 6C). Briefly, corneas were fixed, sectioned across the defect, and stained by hematoxylin and eosin. Pathology of corneal epithelium (EP); Bowman's membrane (BM); Stroma (ST); Descenet's membrane (DM); Endothelium (EN) was evaluated. Remarkably, the corneal epithelium of the LSI treatment group showed complete recovery with a smooth, reconstituted surface, absent of inflammation. While the fluorescein test revealed partial resistance to staining at 24 h in the SI group, the regenerated corneal epithelium did not complete differentiation as illustrated by a rough, irregular ocular surface (black arrows).

Having demonstrated that the mitogenic lacritin protein remains active when decorated on a protein polymer nanoparticle, we next investigated whether ELP-mediated particle assembly is required to achieve this result. To address the significance of ELP assembly *in vivo,* the efficacy of LSI nanoparticles can be directly

compared with a thermally non-responsive lacritin fusion protein called LS96 (Table 1). Both LSI and LS96 contain the lacritin sequence followed by an ELP containing 96 total pentameric repeats; however, the ELP previously characterized as S96[35, 52] does not phase separate until above physiological temperatures. Optical density measurements, in fact, revealed that LS96 does not display any observable phase transitions in phosphate buffered saline (Fig. 7A). In addition, DLS confirmed that LSI has a much larger hydrodynamic radius than LS96 at 37 °C (Fig. 7B). Using these two related formulations of lacritin ELPs, the corneal defect study in NOD mice was both to confirm the ability of LSI to close the epithelium after 12 h and compare this closure with that of LS96. To better evaluate our experimental observation, we further increased the sample size to eight mice per group, with all right eyes receiving the abrasion procedure. Interestingly, LSI healed the abrasion wound significantly ($p<0.05$) faster than the non thermo-responsive LS96 fusion (Fig. 7D). This finding directly supports the contention that ELP-mediated assembly is involved with the enhancement of LSI. To the best of our knowledge, this is the first definitive study showing that ELP-mediated assembly can be used to boost the activity of a mitogenic peptide.

4. Conclusions

To accelerate the corneal wound healing process, this manuscript describes a multivalent ELP nanoparticle as a means of delivering a candidate biopharmaceutical, the mitogen lacritin, to the ocular surface. This lacritin ELP fusion, LSI, displays thermo-responsive self-assembly properties similar to the unmodified SI nanoparticle and presents accessible lacritin at its corona at physiologically relevant temperatures. LSI nanoparticles trigger calcium dependent cell signaling, internalize into cells, and facilitate scratch closure in monolayers of a human corneal epithelial cell line (HCE-Ts). When topically applied on the ocular surface of NOD mice following removal of the corneal epithelium, LSI nanoparticles promoted faster wound healing compared to SI and untreated groups. Most importantly, the LSI nanoparticles produce faster regeneration of the corneal epithelium compared to a control lacritin ELP fusion, called LS96, that does not undergo thermally-mediated assembly. Overall, this study highlights the potential of ELPs as nanoparticle scaffolds to effectively deliver protein therapeutics to the ocular surface and repair abrasion wounds. This strategy may have utility in developing other candidate peptides into biopharmaceuticals. To maximize the conversion of biologically active peptides into drugs, this manuscript suggests that it may be beneficial to induce their multivalent presentation on a nanoparticle; furthermore, ELP protein polymers have emerged as a new strategy to directly bioengineer these particles at the genetic level.

Acknowledgements

This study is supported by the USAMRMC/TATRC grant W81XWH1210538, NIH EY011386, and the USC Whittier foundation. The authors appreciate important discussions regarding the study with Dr. Gordon W. Laurie and Dr. Robert L. McKown. The authors thank Frances Yarber and Dr. Gabriel Gordon for technical support of the animal studies. The authors thank Dr. Tianyi Jiang for cloning the LS96 gene and Dr. Benjamin Droese's technical support in cloning the LSI gene.

Notes and references

1. R. I. Haddadin, G. K. Vora and J. Chodosh, *International ophthalmology clinics*, 2013, **53**, 23-32.
2. K. Kimura, S. Teranishi, K. Fukuda, K. Kawamoto and T. Nishida, *Investigative ophthalmology & visual science*, 2008, **49**, 565-571.
3. K. Suzuki, J. Saito, R. Yanai, N. Yamada, T. Chikama, K. Seki and T. Nishida, *Prog Retin Eye Res*, 2003, **22**, 113-133.
4. M. V. Netto, R. R. Mohan, R. Ambrosio, A. E. K. Hutcheon, J. D. Zieske and S. E. Wilson, *Cornea*, 2005, **24**, 509-522.
5. B. Klenkler and H. Sheardown, *Exp Eye Res*, 2004, **79**, 677-688.
6. T. Kitazawa, S. Kinoshita, K. Fujita, K. Araki, H. Watanabe, Y. Ohashi and R. Manabe, *Investigative ophthalmology & visual science*, 1990, **31**, 1773-1778.
7. C. Scardovi, G. P. Defelice and A. Gazzaniga, *Ophthalmologica*, 1993, **206**, 119-124.

8. C. Sotozono, T. Inatomi, M. Nakamura and S. Kinoshita, *Investigative ophthalmology & visual science*, 1995, **36**, 1524-1529.
9. A. Lambiase, P. Rama, S. Bonini, G. Caprioglio and L. Aloe, *New Engl J Med*, 1998, **338**, 1174-1180.
10. H. M. Leibowitz, S. Morello, Jr., M. Stern and A. Kupferman, *Archives of ophthalmology*, 1990, **108**, 734-737.
11. J. M. Embil, K. Papp, G. Sibbald, J. Tousignant, J. M. Smiell, B. Wong and C. Y. Lau, *Wound repair and regeneration : official publication of the Wound Healing Society [and] the European Tissue Repair Society*, 2000, **8**, 162-168.
12. R. Karnati, D. E. Laurie and G. W. Laurie, *Exp Eye Res*, 2013, **117**, 39-52.
13. S. Sanghi, R. Kumar, A. Lumsden, D. Dickinson, V. Klepeis, V. Trinkaus-Randall, H. F. Frierson and G. W. Laurie, *J Mol Biol*, 2001, **310**, 127-139.
14. N. Wang, K. Zimmerman, R. W. Raab, R. L. McKown, C. M. L. Hutnik, V. Talla, M. F. Tyler, J. K. Lee and G. W. Laurie, *J Biol Chem*, 2013, **288**, 18146-18161.
15. M. M. Feng, J. Baryla, H. Liu, G. W. Laurie, R. L. McKown, N. Ashki, D. Bhayana and C. M. Hutnik, *Current eye research*, 2014.
16. Y. H. Zhang, N. N. Wang, R. W. Raab, R. L. McKown, J. A. Irwin, I. Kwon, T. H. van Kuppevelt and G. W. Laurie, *J Biol Chem*, 2013, **288**, 12090-12101.
17. P. S. Ma, S. L. Beck, R. W. Raab, R. L. McKown, G. L. Coffman, A. Utani, W. J. Chirico, A. C. Rapraeger and G. W. Laurie, *J Cell Biol*, 2006, **174**, 1097-1106.
18. J. C. Lang, *Adv Drug Deliver Rev*, 1995, **16**, 39-43.
19. S. K. Sahoo, F. Diinawaz and S. Krishnakumar, *Drug Discov Today*, 2008, **13**, 144-151.
20. Y. Diebold, M. Jarrin, V. Saez, E. L. Carvalho, M. Orea, M. Calonge, B. Seijo and M. J. Alonso, *Biomaterials*, 2007, **28**, 1553-1564.
21. R. C. Nagarwal, S. Kant, P. N. Singh, P. Maiti and J. K. Pandit, *Journal of controlled release : official journal of the Controlled Release Society*, 2009, **136**, 2-13.
22. M. P. Monopoli, C. Aberg, A. Salvati and K. A. Dawson, *Nature nanotechnology*, 2012, **7**, 779-786.
23. J. A. Hubbell and A. Chilkoti, *Science*, 2012, **337**, 303-305.
24. D. E. Meyer and A. Chilkoti, *Nature biotechnology*, 1999, **17**, 1112-1115.
25. D. L. Nettles, A. Chilkoti and L. A. Setton, *Adv Drug Deliv Rev*, 2010, **62**, 1479-1485.
26. A. Chilkoti, T. Christensen and J. A. MacKay, *Current opinion in chemical biology*, 2006, **10**, 652-657.
27. P. Shi, S. Aluri, Y. A. Lin, M. Shah, M. Edman, J. Dhandhukia, H. G. Cui and J. A. MacKay, *Journal of Controlled Release*, 2013, **171**, 330-338.
28. G. Sun, P. Y. Hsueh, S. M. Janib, S. Hamm-Alvarez and J. A. MacKay, *Journal of controlled release : official journal of the Controlled Release Society*, 2011, **155**, 218-226.
29. D. J. Callahan, W. E. Liu, X. H. Li, M. R. Dreher, W. Hassouneh, M. Kim, P. Marszalek and A. Chilkoti, *Nano Lett*, 2012, **12**, 2165-2170.
30. S. R. MacEwan and A. Chilkoti, *Nano Lett*, 2012, **12**, 3322-3328.
31. S. R. Aluri, P. Shi, J. A. Gustafson, W. Wang, Y. A. Lin, H. G. Cui, S. L. Liu, P. S. Conti, Z. B. Li, P. S. Hu, A. L. Epstein and J. A. MacKay, *ACS nano*, 2014, **8**, 2064-2076.
32. C. C. Liang, A. Y. Park and J. L. Guan, *Nat Protoc*, 2007, **2**, 329-333.
33. A. J. Simnick, M. Amiram, W. Liu, G. Hanna, M. W. Dewhirst, C. D. Kontos and A. Chilkoti, *Journal of controlled release : official journal of the Controlled Release Society*, 2011, **155**, 144-151.
34. S. R. Macewan and A. Chilkoti, *Nano letters*, 2012, **12**, 3322-3328.
35. S. M. Janib, M. Pastuszka, S. Aluri, Z. Folchman-Wagner, P. Y. Hsueh, P. Shi, A. Yi, H. Cui and J. A. Mackay, *Polymer chemistry*, 2014, **5**, 1614-1625.
36. M. J. Berridge and G. Dupont, *Current opinion in cell biology*, 1994, **6**, 267-274.
37. G. C. Churchill, M. M. Atkinson and C. F. Louis, *Journal of cell science*, 1996, **109 (Pt 2)**, 355-365.
38. Y. J. Sung, Z. Sung, C. L. Ho, M. T. Lin, J. S. Wang, S. C. Yang, Y. J. Chen and C. H. Lin, *Experimental cell research*, 2003, **287**, 209-218.
39. K. Arakisasaki, Y. Ohashi, T. Sasabe, K. Hayashi, H. Watanabe, Y. Tano and H. Handa, *Investigative ophthalmology & visual science*, 1995, **36**, 614-621.
40. J. Wang, N. Wang, J. Xie, S. C. Walton, R. L. McKown, R. W. Raab, P. Ma, S. L. Beck, G. L. Coffman, I. M. Hussaini and G. W. Laurie, *The Journal of cell biology*, 2006, **174**, 689-700.
41. M. M. Feng, J. Baryla, H. Liu, G. W. Laurie, R. L. McKown, N. Ashki, D. Bhayana and C. M. L. Hutnik, *Curr Eye Res*, 2014, **39**, 604-610.

42. R. Weissleder, K. Kelly, E. Y. Sun, T. Shtatland and L. Josephson, *Nature biotechnology*, 2005, **23**, 1418-1423.
43. A. Verma and F. Stellacci, *Small*, 2010, **6**, 12-21.
44. W. Jiang, B. Y. S. Kim, J. T. Rutka and W. C. W. Chan, *Nat Nanotechnol*, 2008, **3**, 145-150.
45. P. M. Dubois, J. Stepinski, J. Urbain and C. H. Sibley, *Eur J Immunol*, 1992, **22**, 851-857.
46. S. Barua, J. W. Yoo, P. Kolhar, A. Wakankar, Y. R. Gokarn and S. Mitragotri, *P Natl Acad Sci USA*, 2013, **110**, 3270-3275.
47. I. A. Darby, T. Bisucci, T. D. Hewitson and D. G. MacLellan, *Int J Biochem Cell B*, 1997, **29**, 191-200.
48. J. Rich and J. C. Lee, *Diabetes*, 2005, **54**, 2904-2910.
49. K. Y. Lee, M. C. Peters, K. W. Anderson and D. J. Mooney, *Nature*, 2000, **408**, 998-1000.
50. R. Mohan, S. K. Chintala, J. C. Jung, W. V. L. Villar, F. McCabe, L. A. Russo, Y. Lee, B. E. McCarthy, K. R. Wollenberg, J. V. Jester, M. Wang, H. G. Welgus, J. M. Shipley, R. M. Senior and M. E. Fini, *J Biol Chem*, 2002, **277**, 2065-2072.
51. G. M. Gordon, J. S. Austin, A. L. Sklar, W. J. Feuer, A. J. Lagier and M. E. Fini, *J Cell Physiol*, 2011, **226**, 1461-1470.
52. W. Wang, P. G. Sreekumar, V. Valluripalli, P. Shi, J. Wang, Y. A. Lin, H. Cui, R. Kannan, D. R. Hinton and J. A. Mackay, *Journal of controlled release : official journal of the Controlled Release Society*, 2014.

Table 1. Nomenclature, amino acid sequence, and physicochemical property of expressed proteins

Protein Label	*Amino Acid Sequence	**Expected M.W.(kDa)	***Observed M.W. (kDa)	T_{t1} (°C)	T_{t2} (°C)
SI	$G(VPGSG)_{48}(VPGIG)_{48}Y$	39.65	39.54	32.3	73.1
LSI	GEDASSDSTGADPAQEAGTSKPNEEISGPAEPASPPETTTTAQE TSAAAVQGTAKVTSSRQELNPLKSIVEKSILLTEQALAKAGKGMH GGVPGGKQFIENGSEFAQKLLKKFSLLKPWAGLVPRGSG $(VPGSG)_{48}(VPGIG)_{48}Y$	52.61	52.21	18.7	n.d.
LS96	GEDASSDSTGADPAQEAGTSKPNEEISGPAEPASPPETTTTAQE TSAAAVQGTAKVTSSRQELNPLKSIVEKSILLTEQALAKAGKGMH GGVPGGKQFIENGSEFAQKLLKKFSLLKPWAGLVPRGSG $(VPGSG)_{96}Y$	51.36	51.15	n.d.	n.d.

*After the start codon, a glycine spacer was added during cloning which is not present on human lacritin

**Expected M.W.(kDa) was calculated by DNAStar Lasergene Editseq

***Observed M.W. (kDa) was measured by MALDI-TOF

****T_t (°C) was defined at the point of the maximum first derivative of 25 μM protein solution turbidity change at 350 nm in Phosphate Buffer Saline (PBS). n.d. not detected.

Figure 1. Construction of a thermo-responsive nanoparticle decorated with a mitogenic protein. (**A**) A gene encoding lacritin was fused to an ELP diblock copolymer called SI and expressed as a protein called LSI. LSI undergoes temperature-dependent assembly of a nanoparticle above its phase transition temperature (T_t). (**B**) After purification, gel electrophoresis (SDS-PAGE) was used to confirm the molecular weight for expressed LSI and SI. (**C**) An optical density profile was obtained upon heating purified polymers in phosphate buffered saline (25 μM). SI shows two inflections, where the first represents the assembly of a nanoparticle (T_{t1}) and the second represents the bulk phase separation (T_{t2}) of that nanoparticle. In contrast, LSI shows only a single inflection and does not undergo bulk phase separation. (**D**) Optical density data was compiled to create a concentration-temperature phase diagram for LSI and SI. Dashed lines indicate the fit of T_t to the following equation: $T_t = m \log_{10}[C_{ELP}] + b$ where C_{ELP} is the concentration, m is the slope, and b is the transition temperature at 1 μM. For T_t of LSI, b = 19.69 °C and m = -0.64 °C (Log 10[μM])$^{-1}$. For T_{t1} of SI, b = 65.06 °C, m = -22.56 °C (Log 10[μM])$^{-1}$. For T_{t2} of SI, b = 77.98 °C, m = -3.72 °C (Log 10[μM])$^{-1}$.

Figure 2. LSI and SI assemble nanoparticles at physiological temperatures. (**A**) Dynamic Light Scattering (DLS) was performed during heating, which shows that SI assemble nanoparticles with a R_h of 22.3 ± 1.1 nm at 37 °C. Below T_{t1} LSI form 30-40 nm structures; however, above T_t these reconstitute into stable 147 ± 36 nm nanoparticles at 37 °C. (**B,C**) TEM images of (**B**) SI and (**C**) LSI nanoparticles, with average diameter of 36.5 ± 5.8 nm and 67.1 ± 11.5 nm accordingly. The scale bar represents 100 nm.

Figure 3. LSI nanoparticles stimulate Ca^{2+}- mediated signaling in corneal epithelial cells. HCE-T cells were treated with Fluo-4AM to detect calcium-mediated signaling and imaged using live cell confocal microscopy. The upper images are representative of the peak intensity following the administration of either LSI or SI (40 μM). The lower plot presents the fluorescence intensity as a function of time in ten individual cells. The percentage change in fluorescence intensity, F_t, compared to the initial time point, F_0, was estimated as follows: $F_t = (F_t - F_0)/F_0 \times 100\%$. (**A**) LSI nanoparticles were administered twice, each time triggering a 3-6 fold increase in intracellular Ca^{2+}. (**B**) In contrast, the same concentration of SI did not elicit a significant effect (****p<0.0001, n=10). The scale bar represents 20 μm. Maximum fluorescence intensity changes were analyzed using an un-paired t-test.

Figure 4. LSI nanoparticles mediate scratch closure in corneal epithelial cells. HCE-T cells were grown to confluence on tissue culture polystyrene, scratched, and imaged for 24 h to observe the rate of closure. (**A**) At low concentrations, 10 nM LSI nanoparticles completely closed the scratch. This finding was similar to that obtained by a positive control containing epidermal growth factor (EGF) (5 ng/ml) and bovine pituitary extract (BPE) (50 μg/ml). In contrast, the no treatment group (medium only) failed to close the scratch. The scale bar represents 100 μm. (**B**) The scratch closure at 24 h was quantified to show that LSI nanoparticles induce an effect similar to control EGF and BPE. The no treatment group retained more than 80 % of initial scratch width. Each treatment condition was performed in triplicate and four representative distances in each well were measured for statistical analysis (***p<0.001, n=12). Data were analyzed by a blind reviewer. Images were quantified using ImageJ and analyzed using one-way ANOVA followed by Tukey's post-test.

Figure 5. Lacritin mediates nanoparticle uptake in corneal epithelial cells. HCE-T cells were incubated with rhodamine labeled LSI or SI nanoparticles and imaged using confocal microscopy. (**A**) Representative images show time dependent uptake of LSI while SI nanoparticles do not internalize to the same degree. Red: rhodamine labeled LSI and SI; Blue: DAPI staining of nuclei. The scale bar represents 10 μm. (**B**) For cell uptake quantification, each treatment was repeated three times and three representative cells on each plate were chosen for analysis purpose. Remarkably, LSI exhibits significantly higher uptake level than SI (****p<0.0001, n=9) at 60 m. Images were quantified using ImageJ and analyzed via two-way ANOVA followed by a Bonferroni post-hoc t-test.

Figure 6. Lacritin-decorated nanoparticles heal abrasions in the corneal epithelium of mice. An algerbrush II was used to create a 2 mm defect in the corneal epithelium of female non-obese diabetic (NOD) mice, which were monitored using fluorescein staining at 0, 12 and 24 h with or without treatment by LSI, SI, and a positive control EGF+BPE. (**A**) Representative images showing the time-lapse healing of the defect on the corneal epithelium. (**B**) The area of the wounds as a percent of the initial wound area (PctArea) was determined by a blind reviewer to ensure objectivity. A Kruskal-Wallis non-parametric test was used to compare groups. These revealed that LSI at both 12 and 24 h significantly (***p=0.001, n=4) decreased the percentage of initial wound area (PctArea) compared to SI, EGF+BPE, and no treatment groups. (**C**) After 24 h, corneas were fixed, sectioned across the defect, and stained by hematoxylin and eosin. The corneal epithelium of the LSI treatment group revealed normal pathology, absent of inflammation. Although reduced fluorescein staining was observed at late times in the SI group, the epithelium did not recover fully, as evidenced by its irregular surface (black arrows). EP: epithelium; BM: Bowman's membrane; ST: Stroma; DM: Descenet's membrane; EN: Endothelium.

Figure 7. ELP-mediated assembly is essential for the *in vivo* activity of LSI nanoparticles. To determine whether the potency of LSI nanoparticles depends on ELP-mediated assembly of SI, a control lacritin fusion called LS96 (Table 1) was expressed. (**A**) Optical density measurements confirmed that LS96 lacks any detectable phase transitions at 25 μM in phosphate buffer saline (PBS). (**B**) Under the same conditions, Dynamic Light Scattering (DLS) was performed at 37 °C, which confirmed that LSI assembles nanoparticles with a R_h of 147.0 ± 35.8 nm, while LS96 produced particles with a R_h of 37.0 ± 8.8 nm, which is similar to that observed for LSI below T_t (Fig. 2A). (**C**) A 2 mm corneal defect was induced in female NOD mice, treated with LSI or LS96, stained by fluorescein at 12 h, and quantified by a blind reviewer. A representative image shows superior integrity of the ocular surface treated with LSI after 12 h. (**D)** Comparison of the PctArea was made by the non-parametric Mann-Whitney U test, which confirms that LSI at 12 h significantly decreases the wound area compared to LS96 (*p<0.05, n=8).

Figure Abstract

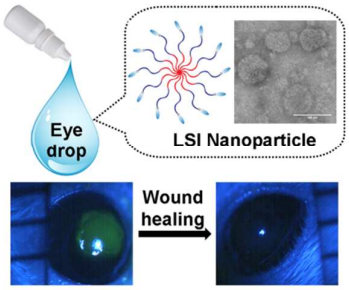

Protein polymer nanoparticles decorated with the mitogenic human tear protein, lacritin, heal a defect in the corneal epithelium faster than a soluble control peptide.

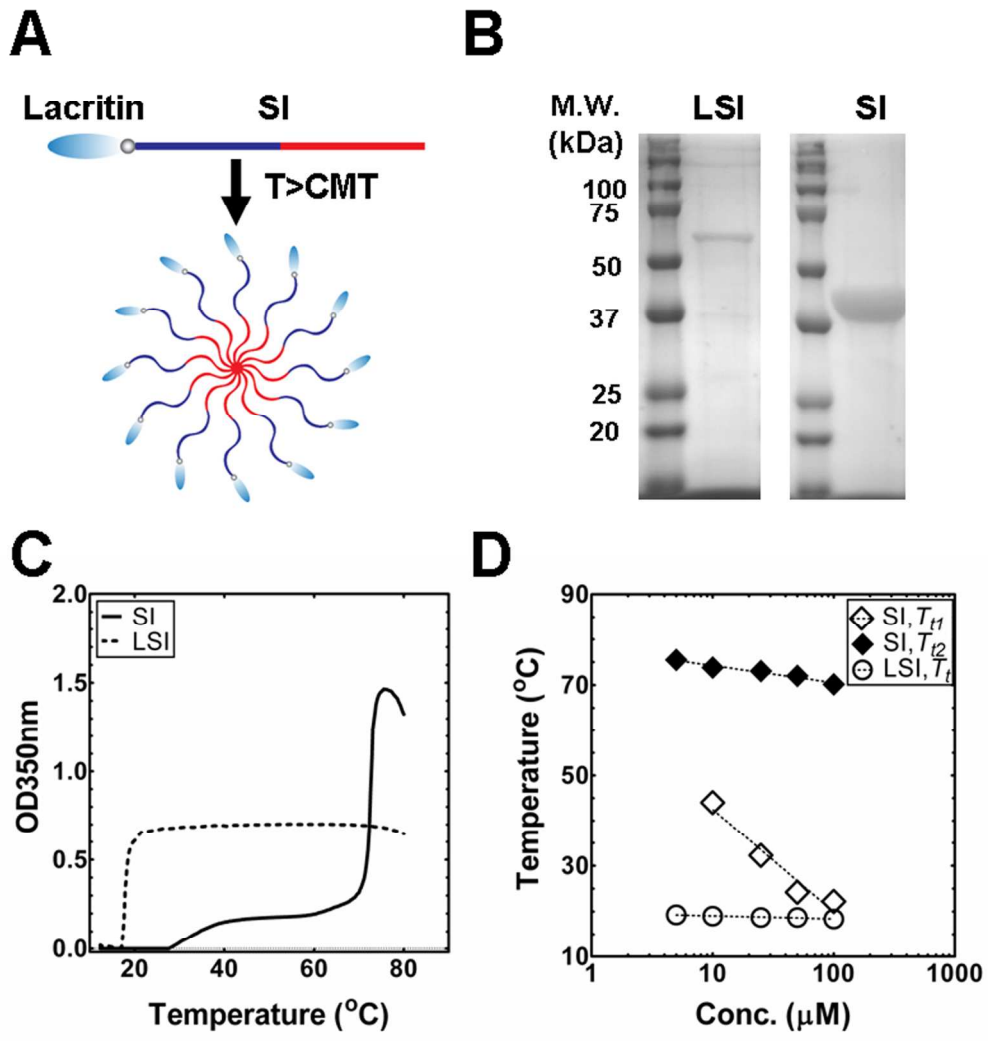

152x159mm (300 x 300 DPI)

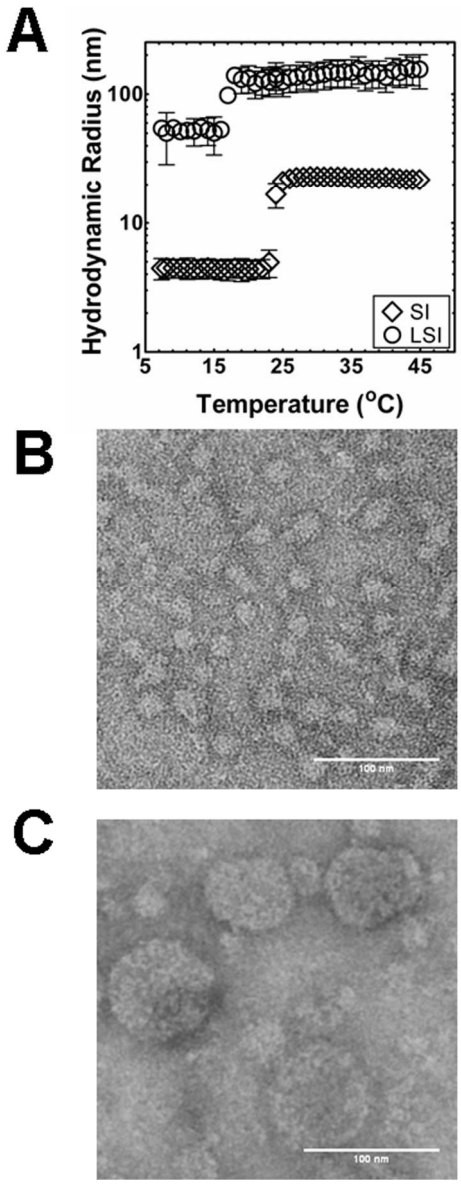

177x440mm (300 x 300 DPI)

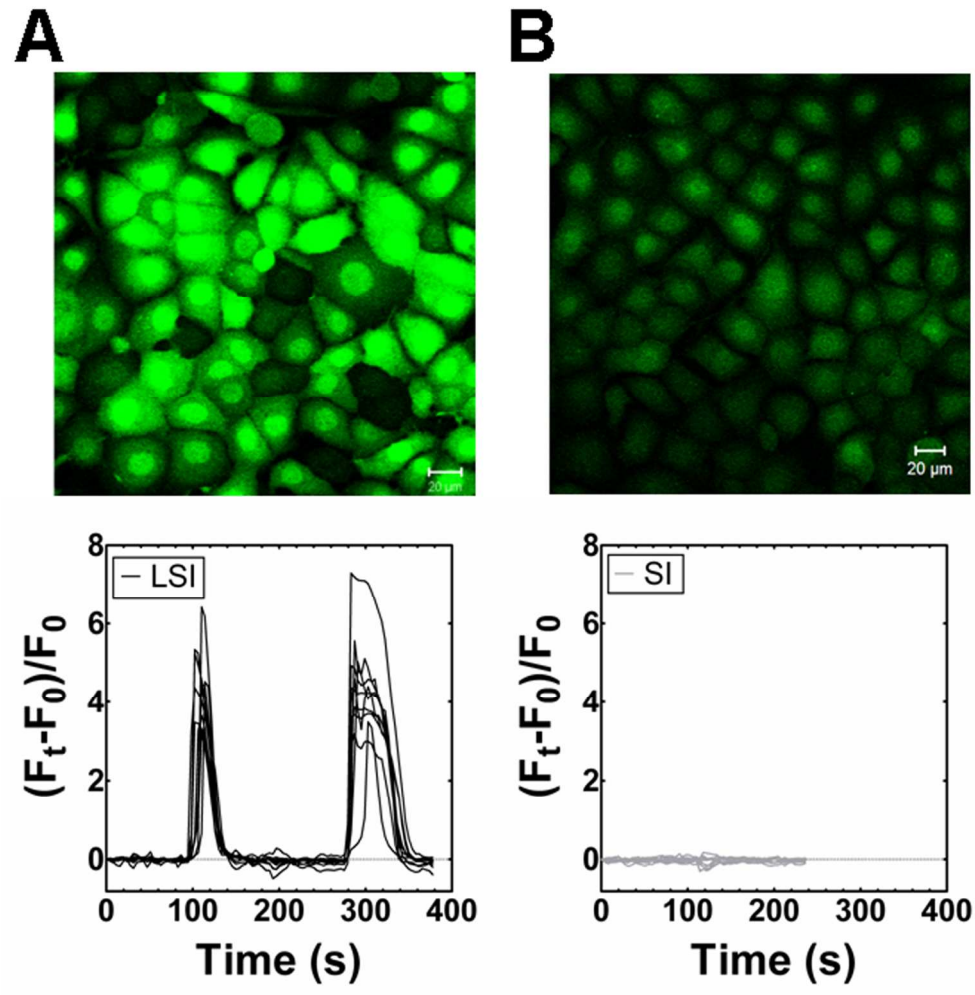

152x152mm (300 x 300 DPI)

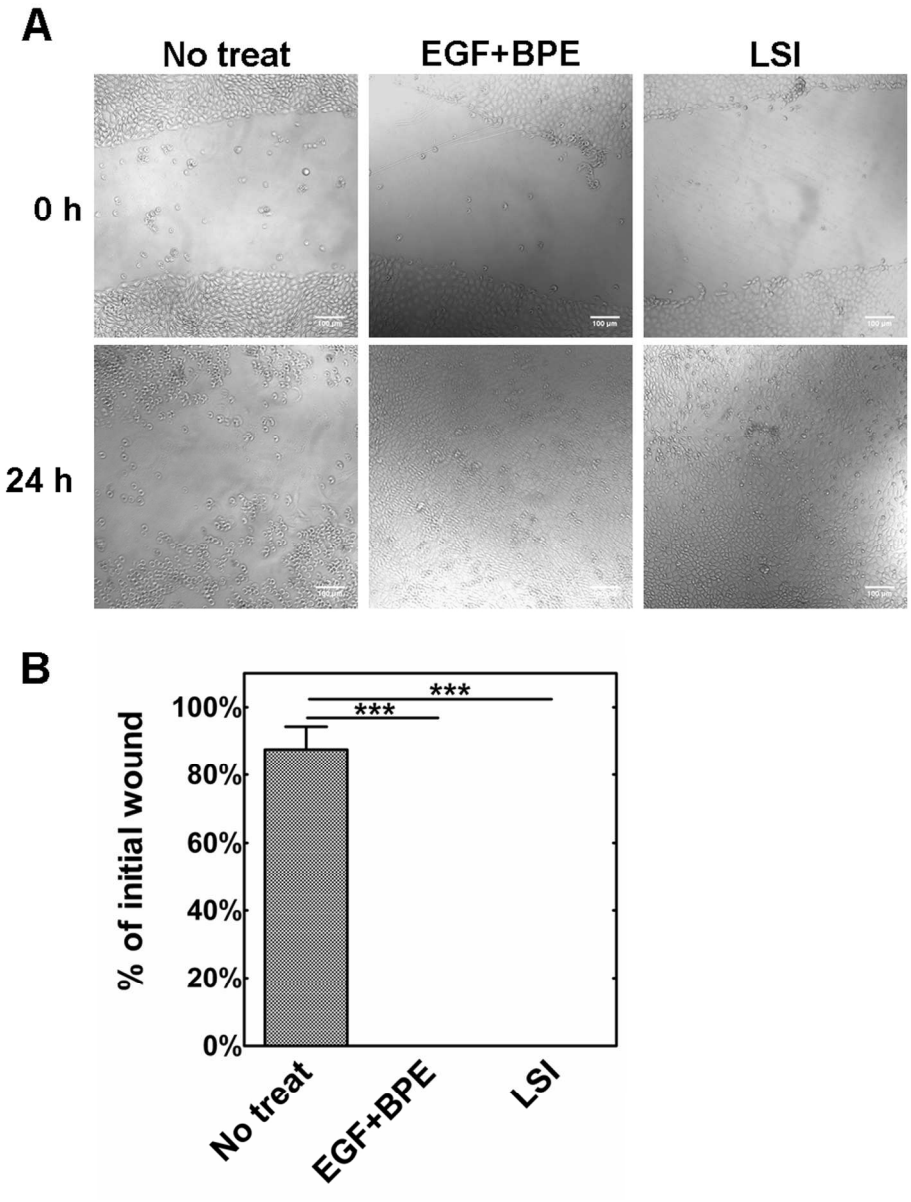

152x194mm (300 x 300 DPI)

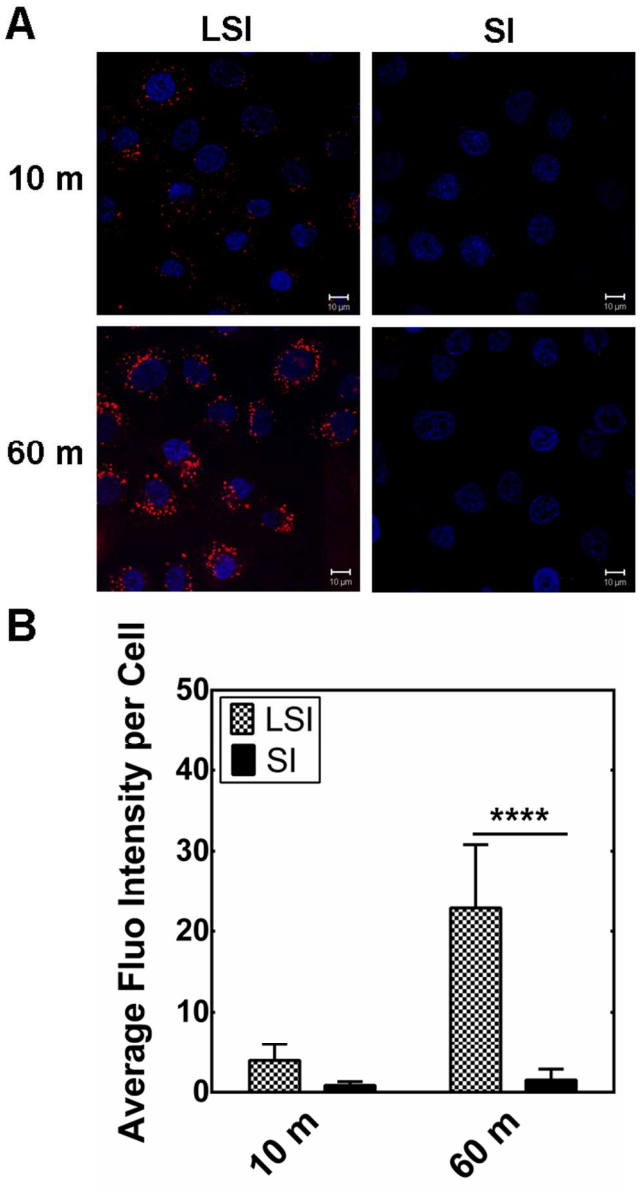

139x255mm (300 x 300 DPI)

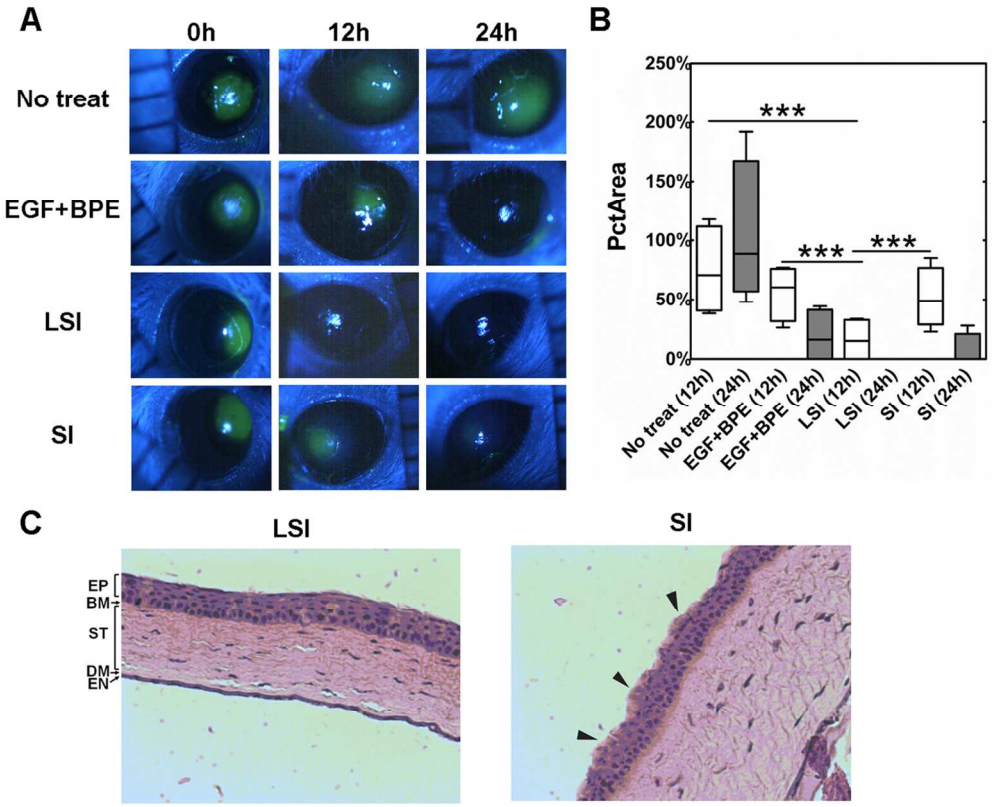

123x100mm (300 x 300 DPI)

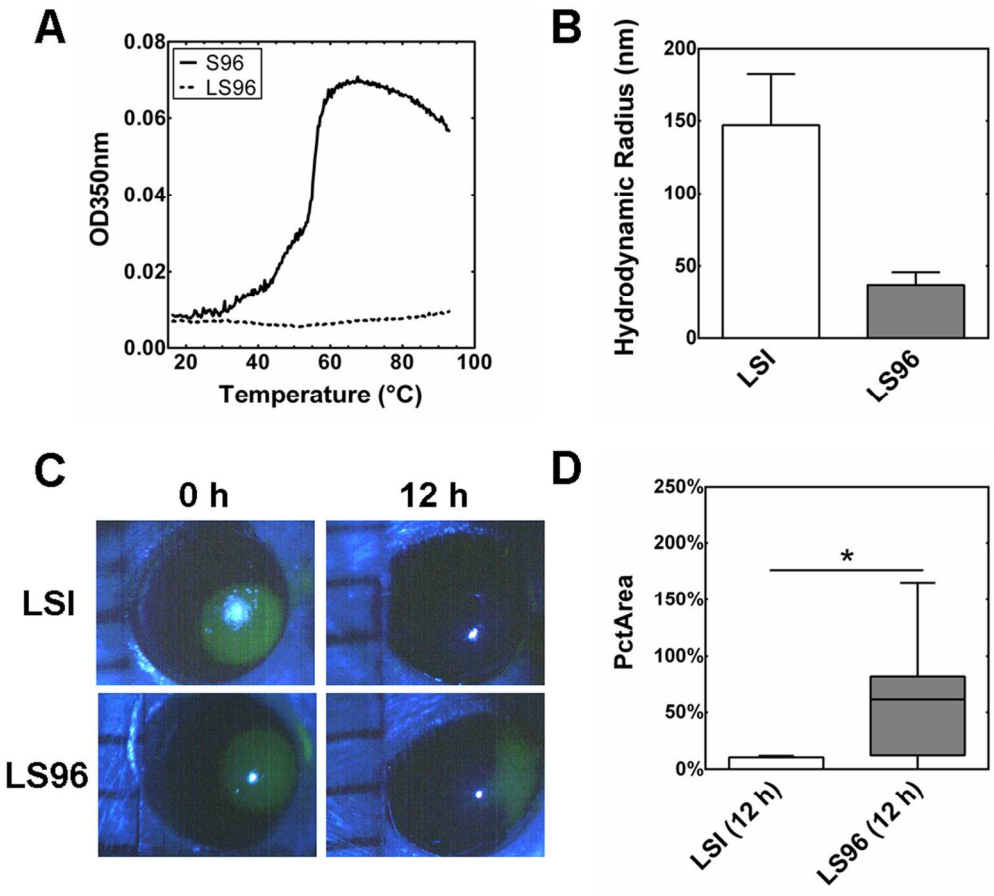

136x123mm (300 x 300 DPI)